Analytical Biochemistry 550 (2018) 72–83

Contents lists available at ScienceDirect

Analytical Biochemistry

journal homepage: www.elsevier.com/locate/yabio

Characterization of therapeutic antibodies in the presence of human serum proteins by AU-FDS analytical ultracentrifugation

Robert T. Wright[a], David B. Hayes[b], Walter F. Stafford[c], Peter J. Sherwood[d], John J. Correia[a,*]

[a] Department of Biochemistry, University of Mississippi Medical Center, Jackson, MS, 39216, USA
[b] Biotherapeutics Discovery Research, Boehringer Ingelheim, Ridgefield, CT, 06877, USA
[c] Department of Systems Biology, Harvard Medical School, Boston, MA, 02115, USA
[d] Interactive Technology, Oakland, CA, 94602, USA

ARTICLE INFO

Keywords:
AUC – analytical ultracentrifugation
AU-FDS – Aviv fluorescence detection system
SV – sedimentation velocity
k_s - hydrodynamic nonideality
$2BM_1$ – thermodynamic nonideality

ABSTRACT

The preclinical characterization of biopharmaceuticals seeks to determine the stability, state of aggregation, and interaction of the antibody/drug with other macromolecules in serum. Analytical ultracentrifugation is the best experimental method to understand these factors. Sedimentation velocity experiments using the AU-FDS system were performed in order to quantitatively characterize the nonideality of fluorescently labeled therapeutic antibodies in high concentrations of human serum proteins. The two most ubiquitous serum proteins are human serum albumin, HSA, and γ-globulins, predominantly IgG. Tracer experiments were done pairwise as a function of HSA, IgG, and therapeutic antibody concentration. The sedimentation coefficient for each fluorescently labeled component as a function of the concentration of the unlabeled component yields the hydrodynamic nonideality (k_s). This generates a 3x3 matrix of k_s values that describe the nonideality of each pairwise interaction. The k_s matrix is validated by fitting both 2:1 mixtures of HSA (1–40 mg/ml) and IgG (0.5–20 mg/ml) as serum mimics, and human serum dilutions (10–100%). The data are well described by SEDANAL global fitting with the k_s nonideality matrix. The k_s values for antibodies are smaller than expected and appear to be masked by weak association. Global fitting to a k_s and K_2 model significantly improves the fits.

Introduction

The development of therapeutic protein drugs (antibodies, drug delivery vectors, *etc.*), requires the use of numerous orthogonal experimental techniques to characterize the purity, heterogeneity, and association or aggregation properties of the drug [1,2]. These techniques must determine how a potential therapeutic protein will behave in the relevant physiological environment. For protein therapeutics the immediate physiological environment is often the blood stream into which the drugs are delivered directly. How the therapeutic antibody will interact with the proteins in human blood and how it binds with its partner at the intended target is crucial. Recombinant antibodies designed as drugs may form dimers or other higher order aggregates [3]. These higher order structures are product-related impurities that result from incorrect heavy or light chain association [4]. Preclinical characterization of therapeutic antibodies seeks to identify the presence of aggregates and potential changes in molecular interactions with the target in human serum upon injection [5]. The most common method in the field for analyzing therapeutic protein aggregation is size-exclusion chromatography (SEC) [3,6–8]. By separating a solution according to the size of the components, SEC enables the detection and quantification of both small and large molecular species (free chains and aggregates). However, a weakness of SEC is the inability to determine accurately the presence of large aggregates due to nonspecific interactions between the biopharmaceutical and the column material [3,9].

The Food and Drug Administration (FDA) and industry standards require orthogonal methods as a component of the analysis of therapeutic proteins, with SV analytical ultracentrifugation being the method most commonly chosen for the biophysical characterization of aggregates [2,10,11]. Analytical ultracentrifugation (AUC) allows for the determination of the size, shape, state of aggregation, and reversible interaction between macromolecules. The most common use of AUC for the study of therapeutic antibodies is the detection of aggregation [3,12]. Arthur et al. [13] performed studies looking at the variability of detecting aggregates of therapeutic antibodies by sedimentation velocity in ideal solution conditions. They concluded that, while AUC studies are helpful as a validation tool, there is relatively high variability as compared to SEC. Other work by Arakawa et al. [7] found that sedimentation velocity by AUC could detect the presence of monoclonal antibody aggregates with greater sensitivity than SEC. When it comes to

* Corresponding author.
E-mail address: jcorreia@umc.edu (J.J. Correia).

https://doi.org/10.1016/j.ab.2018.04.002
Received 5 March 2018; Received in revised form 4 April 2018; Accepted 5 April 2018
Available online 11 April 2018
0003-2697/

accurately and consistently detecting protein aggregation, the generally held consensus is that SEC is the gold standard while AUC provides an orthogonal method [2]. The basis of these contrasting opinions is in part due to systematic errors during SV-AUC including misalignment of cells, defects in centerpieces, and calibration uncertainty [12–14]. The clear advantage of AUC is the ability to perform experiments in formulation conditions while avoiding significant dilution effects and interactions with a large chromatography matrix surface area. These advantages extend to other areas such as lead candidate selection, formulation development, and product characterization where AUC offers benefits over other experimental techniques [15].

A goal of biotech developers of therapeutic proteins is to perform preclinical studies in serum and plasma. To understand the influence of serum on the hydrodynamic behavior of protein drugs, AUC must be performed with the Aviv AU-FDS [16]. The AU-FDS utilizes confocal fluorescence optics and avoids nonlinear, saturating absorbance or refractometric response. This refractometric response typically manifests as Schlieren effects due to the bending of light in the steep gradient generated by a sedimentation velocity experiment [17–19]. These artifacts prevent accurate determination of the sedimentation coefficient at high concentrations. Thus, AU-FDS is an invaluable tool for detecting molecular behavior in crowded environments [20,21]. Some early studies discovered difficulty fitting FDS sedimentation velocity data to the Lamm equation when performing c(s) analysis for highly concentrated solutions [5,22,23]. Working at high concentrations with the AU-FDS it was found that Lamm equation modeling by c(s) produced systematic residuals. The use of model independent methods like DCDT or WDA appears to avoid these issues for single sample analysis [24–26]. Recent advances in AUC data analysis software such as SEDANAL, however, have overcome these difficulties and complex Lamm equation global modeling (including nonideality, aggregation and association) of high concentration data is now possible [27–30].

Previous work in our lab [29] focused on AU-FDS AUC studies of trace quantities of Elastin-Like Polypeptides (ELP) in BSA and bovine IgG solutions to mimic and approximate AUC studies in serum solutions. These tracer experiments may be categorized as either NUTS or BOLTS experiments [16,21]. Normal use tracer sedimentation (NUTS) allows for the study of dilute concentrations of macromolecules in a solution, while biological on-line tracer sedimentation (BOLTS) characterizes trace amounts of a fluorescently labeled macromolecule in a complex, heterogeneous mixture of molecules. Sedimentation analysis of tracers in human serum qualifies as BOLTS because serum is a highly heterogeneous mixture which contains a high concentration of protein (70–100 g/L). The concentrations of human serum components vary in the literature, but typical values are human serum albumin 34–70 mg/ml, immunoglobulins (predominantly IgG) 5–20 mg/ml, transferrin 3–7 mg/ml, α-1 anti-trypsin 2–4 mg/ml, and serum lipoproteins 1–10 mg/ml. Lipid vesicles can be hundreds of nanometers in size and some float instead of sediment.

Tracer experiments have been used to address the theoretical implications of nonideality [16,31–33]. Sedimentation studies determining nonideality give insight into the slowing and sharpening of the sedimentation boundary of a molecule due to itself or other components. Nonideality studies via sedimentation velocity must account for the sedimentation of a specific molecule as a function of the concentration of all other components in solution. This is described by the empirical expression for a sedimentation coefficient:

$$s_1 = \frac{s_1^0}{1 + k_{11}c_1 + k_{12}c_2 + k_{13}c_3 + \ldots} \quad (1)$$

where s_1 is the sedimentation coefficient of component 1, s_1^0 is the sedimentation coefficient extrapolated to zero concentration of all components, k_{ij} values are the hydrodynamic nonideality terms showing the s(c) dependence for the interacting components, and the c_i terms are the concentrations (mg/ml) of each component.

In this study we characterized the hydrodynamic behavior of two monoclonal antibodies (NIST mAb and golimumab) by sedimentation velocity using the AU-FDS. Tracer experiments were performed to extract hydrodynamic nonideality (k_s) values for pair-wise interactions (k_{ij}) between the therapeutic antibody, human serum albumin, and total human IgG. The nonideality k_{ij} matrix values were then verified by fitting data from sedimentation velocity experiments of a therapeutic antibody in mixtures of HSA and IgG and in a dilution series of human serum samples. The results are discussed in terms of the challenge of also measuring reversible molecular interactions that may mask the nonideality of the solution.

Materials and methods

Materials

The NIST mAb and Golimumab therapeutic antibodies were provided by Boehringer-Ingelheim.[1] A second lot of Golimumab was also purchased from the local UMMC pharmacy. Human serum albumin was purchased from Sigma Aldrich in the “fatty-acid free” form (A3782). For the γ-globulins a heterogeneous mixture of the total IgG serum fraction was obtained from Golden West Biologicals, Inc. (HGG1000). Human serum (pooled and FABP free) was purchased from Fitzgerald Industries International (catalog #90R-109; lot #S13091602). Analytical ultracentrifugation experiments were run in phosphate-buffered saline (PBS; 150 mM NaCl, 2.7 mM KCl, 20 mM Na_2HPO_4, and 1.8 mM KH_2PO_4, pH 7.4) or dilutions of human serum. HSA, IgG and mAbs were stored as stock solutions dialyzed into PBS using Slide-A-Lyzer MINI Dialysis Devices (Thermo Scientific).

Protein labeling

NIST mAb and Golimumab were labeled by Boehringer-Ingelheim and our lab with Alexa-Fluor 488 carboxylic acid, succinimidyl ester (Molecular Probes A20100). Human serum albumin and total human IgG were labeled with fluorescein 5(6)-isothiocyanate (Sigma Aldrich F3651). Thermo Scientific (Alexa-Fluor 488) and Sigma (FITC) protocols for fluorescence labeling were followed. Typically the mAbs had 3-4 Alexa-488 molecules covalently bound per mAb. Total human IgG had ~1 FITC bound per IgG molecule. HSA had ~0.5 FITC bound per HSA.

Density and viscosity measurements

PBS buffer density was measured in an Anton Paar DMA 5000 and DMA 5000 M density meter at 19.69 °C (as calibrated by the method of Liu and Stafford) [34]. The buffer viscosity was estimated with Sednterp [35,36] to be 1.0097 cP.

Analytical ultracentrifugation

All experiments were performed in an Optima XL-A analytical ultracentrifuge. Samples were made at the desired concentration and loaded into double sector cells. The samples were loaded into centrifuge cells equipped with 1.2 cm or 3 mm SedVel50 centerpieces and sapphire windows. The centrifuge cells were placed into an An-60 rotor and the temperature of the AUC was equilibrated to 20 °C for at least 1 h prior to the run. Runs were performed at appropriate speeds for each sample. Total human IgG and therapeutic antibodies were run at 40 K. The HSA experiments were performed at 50 K rpm. For experiments run using the AU-FDS AUC the gain was adjusted to give a signal between 500

[1] NIST mAb (“not for human use”) is now an industry standard that was originally developed against Respiratory Syncytial Virus under the trade name motavizumab; golimumab is an anti-inflammatory directed against TNFα. It was chosen for these studies because it was available at BI for other comparative work.

and 1000 counts, the digital multiplier was always kept at 1, and the focus depth was adjusted to the center of the plateau region [37]. The cell averaging intervals were aligned in the middle of the cell. For data collection five scans were acquired and averaged in radial increments of 50 μm. The meniscus position, r_{min}, was determined by layering BODIPY fluorescent dye (0.1% w/v diluted to 0.05% w/v for 1.2 cm centerpieces and 0.01% w/v for 3 mm centerpieces) in light mineral oil on top of the loaded samples [38]. During global fitting any obvious errors in r_{min} were resolved by floating those values, and the best final fits were typically performed floating all r_{men} values as well as the ratio of aggregated dimer/monomer for each sample. The labeled species was added at ~100–200 nM in the presence of increasing amounts of the unlabeled component. For HSA the concentration of the unlabeled component ranged from 1 mg/ml to 40 mg/ml. IgG runs started at 1 mg/ml and went to 20 mg/ml. The experiments involving the unlabeled therapeutic antibody as the background molecule were run from 1 to 11 mg/ml (NIST mAb) or 1–12 mg/ml (golimumab). Fluorescence experiments involving a labeled therapeutic antibody in the presence of 2:1 mixtures of HSA (1–40 mg/ml) and IgG (0.5–20 mg/ml) concentrations also were conducted.

The hydrodynamic nonideality of the therapeutic antibody and each serum component can be obtained empirically through pair-wise specific experiments. These experiments allow for the determination of the nonideality that a macromolecule has on itself (self-term nonideality) or other components (cross-term nonideality) where component 1 is mAb, component 2 HSA and component 3 IgG.

$$s_1 = \frac{s_1^0}{(1 + k_{11}c_1 + k_{12}c_2 + k_{13}c_3)} \quad (2)$$

$$s_2 = \frac{s_2^0}{(1 + k_{21}c_1 + k_{22}c_2 + k_{23}c_3)} \quad (3)$$

$$s_3 = \frac{s_3^0}{(1 + k_{31}c_1 + k_{32}c_2 + k_{33}c_3)} \quad (4)$$

The self-term nonideality is described by the k_{ii} term where i = i. For the cross-term nonideality the term is denoted as k_{ij} where i ≠ j. The $k_{ij}c_i$ terms can be added for other components present in a more complex system, eg. mAb dimers during fitting. The sedimentation coefficient of the labeled species as a function of the unlabeled species determined for pair-wise interactions for both the self- and cross-term nonideality can be plotted as described by Johnston and Ogston [39]:

$$s_1 = \frac{s_1^0}{1 + k_{11}c_1 + k_{12}c_2} \quad (5)$$

For plotting purposes the relationship can be simplified and rearranged into a linear equation due to the low concentration (100–200 nM) of the labeled component $k_{11}c_1$ which renders it negligible:

$$\frac{1}{s_1} = \frac{1}{s_1^0} + \frac{k_{12}}{s_1^0}c_2 \quad (6)$$

where the y-intercept is $1/s_1^0$ and the slope is the k_{12}/s_1^0 term. The slope gives the hydrodynamic nonideality exerted by the unlabeled component (in this case component 2) on the labeled component (component 1). The k_s value is determined by dividing the slope by the $1/s^0$ value.

Initially the SV data were analyzed using the software program DCDT$^+$ [25]. This was done to determine the meniscus position and to observe the concentration dependence via g(s*) distribution overlays. Wide Distribution Analysis (WDA) is also convenient for this purpose [26,40]. The data then were analyzed using SEDANAL with the meniscus position determined from DCDT$^+$, setting the baseline, and manually choosing the fit range and number of scans to fit. Different fitting models were chosen in order to compare the results of different analysis methods. An A + B + C (three species, non-interacting) model was used to individually extract the sedimentation coefficient of the monomer, dimer and trimer species at each of the six individual concentrations run in the experiment. (The s values for dimers and trimers can be allowed to float or constrained in the equation editor by reasonable assumptions about changes to f/fo, eg $s_{dimer} = n^{2/3} * s_{monomer}$. Typically we found $s_{dimer} = 1.45 * s_{monomer}$ and $s_{trimer} = 2.0 * s_{monomer}$.) All sedimentation coefficient data were converted to $s_{20,w}$ using the conversion factor calculated by DCDT$^+$. The $1/s_{20,w}$ values for the monomer were plotted versus concentration of the background species and a linear fit performed to determine the hydrodynamic nonideality, k_s. This was done using Origin 7.5 (OriginLab, Northampton, MA). Each pairwise experiment was repeated 3–5 times and data are reported as mean ± sd (Tables 1 and 2). SEDANAL internally uses concentration units of mg/ml and thus k_s and $2BM_1$ have units of ml/mg making the products k_sc and 2BMc dimensionless. However, the field tends to use ml/g for k_s and $2BM_1$ [41–46] and thus we plot $1/s_{20,w}$ vs mg/ml but report k_s in units of ml/g to be consistent.

Data were also fit globally using SEDANAL with an A + B + C + k_s model, where component A, B and C correspond to the monomer, dimer and trimer species. Fitting was done using data from six background concentrations for each self-k_s determination and each mAb-IgG or IgG-mAb cross term. To test the validity of the 3 × 3 k_s matrix, the HSA and IgG mixture experiments and the human serum dilution sample experiments also were fit using SEDANAL and holding the matrix values constant while fitting only s_1 and the apparent extinction coefficients. Matrix values (Tables 1 and 2) are entered by right clicking on the k_s value for component A which opens an entry box allowing input of the 3x3 values in units of ml/mg. For these models component 1 is mAb, component 2 is HSA and component 3 is IgG (See Fig. S1, a screen shot of a typical model with the matrix window open.).

Table 1
Summary of k_s values determined by a linear fit of the FDS data in Figs. 1, 3 and 4. The k_s determined from global direct boundary fitting with SEDANAL are shown in parentheses.

	NIST mAb	HSA	Human IgG
NIST mAb	3.1 ± 0.3 (4.2 ± 0.4)	6.5 ± 0.3	1.9 ± 0.1 (2.3 ± 0.04)
HSA	−1.2 ± 0.3	9.4 ± 0.2 (8.2 ± 1.0)	1.0 ± 0.3
Human IgG	2.9 ± 0.2 (4.4 ± 0.4)	8.5 ± 0.3	2.9 ± 0.2 (3.1 ± 0.3)

Results

In order to measure the sedimentation of therapeutic antibodies and serum proteins at concentrations that mimic human serum, FDS experiments were performed. Nine sets of pair-wise experiments were performed to investigate the sedimentation behavior of therapeutic antibodies and serum proteins. These experiments tested the effect of the proteins on themselves (self-nonideality) and the other components (cross-term nonideality).

The self-nonideality of each of the therapeutic antibodies is shown

Table 2
Summary of k_s values determined by a linear fit of the FDS data in Figs. 2–4. The k_s determined from global direct boundary fitting with SEDANAL are shown in parentheses.

	Golimumab	HSA	Human IgG
Golimumab	1.8 ± 0.3 (2.5 ± 0.3)	5.4 ± 0.2	1.1 ± 0.1 (1.3 ± 0.2)
HSA	0.8 ± 0.3	9.4 ± 0.2 (8.2 ± 1.0)	1.0 ± 0.3
Human IgG	1.7 ± 0.2 (2.9 ± 0.1)	8.5 ± 0.3	2.9 ± 0.2 (3.1 ± 0.3)

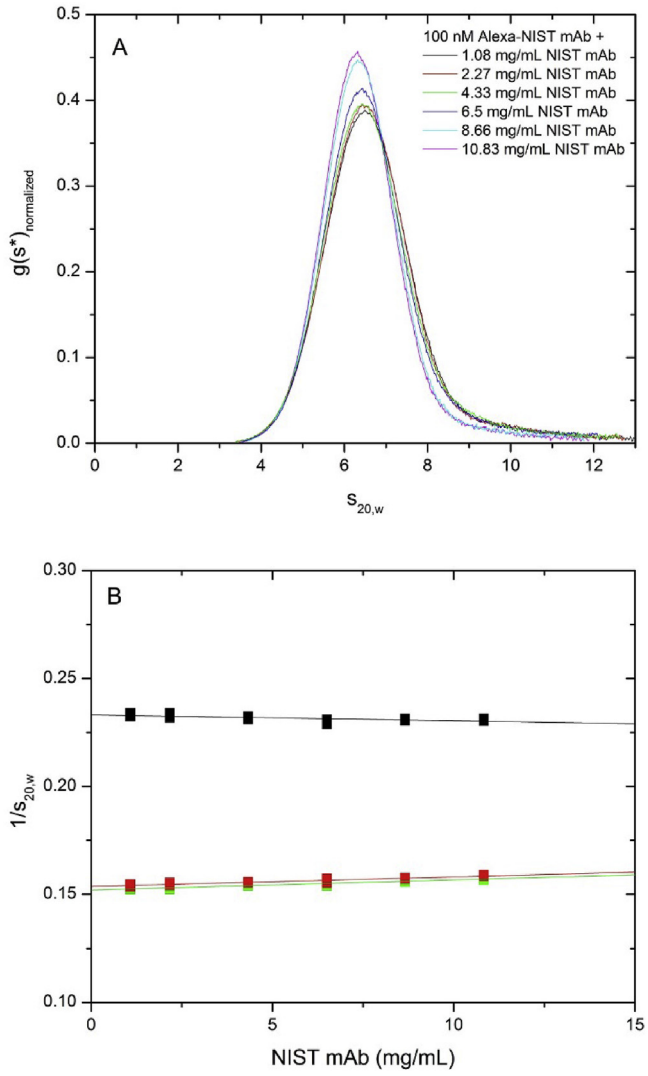

Fig. 1. (a) Normalized g(s*) distributions for 100 nM Alexa-NIST mAb as a function of NIST mAb concentration. (b) Plotting the inverse of the monomer $s_{20,w}$ value of 100 nM FITC-HSA (black), FITC-IgG (red), and Alexa-NIST mAb (green) as a function of NIST mAb concentration (1–12 mg/ml; N = 3). The monomer $s_{20,w}$ values were determined from an A + B + C SEDANAL fit. The slope is equal to the magnitude of the hydrodynamic nonideality (k_s) divided by the sedimentation coefficient extrapolated to zero concentration (s^o).

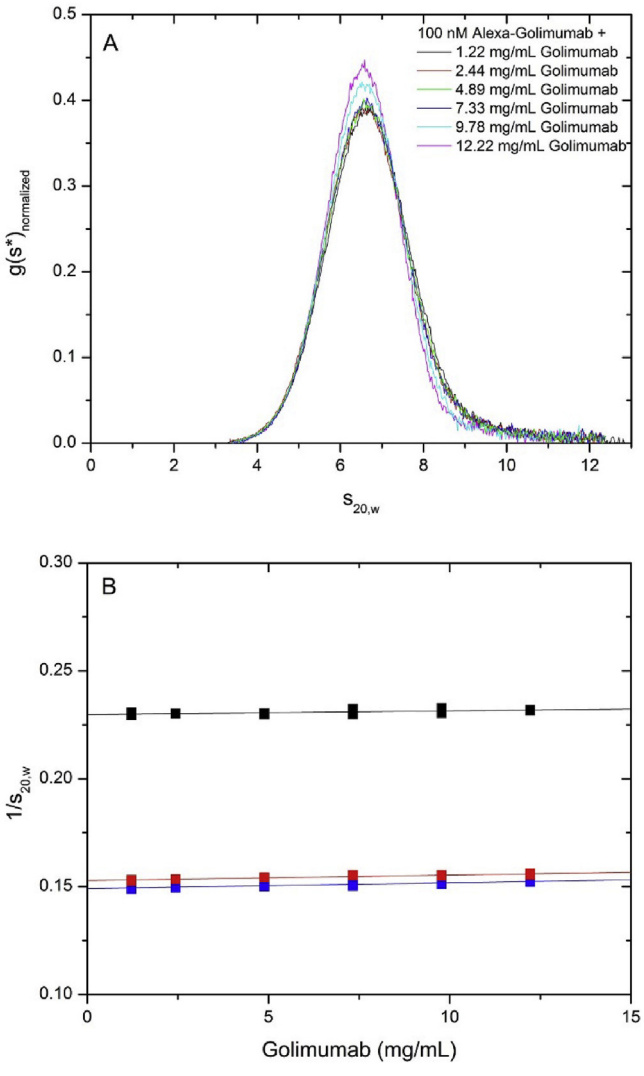

Fig. 2. (a) Normalized g(s*) distributions for 100 nM Alexa-Golimumab as a function of golimumab concentration. (b) Plotting the inverse of the monomer $s_{20,w}$ value of 100 nM FITC-HSA (black), FITC-IgG (red), and Alexa-Golimumab (blue) as a function of Golimumab concentration (1–12 mg/ml). The monomer $s_{20,w}$ values were determined from an A + B + C SEDANAL fit. The slope is equal to the magnitude of the hydrodynamic nonideality (k_s) divided by the sedimentation coefficient extrapolated to zero concentration (s^o).

in Fig. 1 (NIST mAb) and 2 (golimumab). The data reveal the effect on the sedimentation coefficient as a function of increasing concentration. The self-nonideality was measured by running 100 nM of the Alexa-labeled antibody in the presence of increasing concentrations (1–12 mg/ml) of the unlabeled NIST mAb. The decrease in the sedimentation coefficient observed in the g(s*) plot (Figs. 1A and 2A) is caused by hydrodynamic nonideality. The monomer sedimentation coefficients as determined by SEDANAL from the monoclonal antibody data sets were plotted as $1/s_{20,w}$ vs c (mg/ml; Figs. 1B and 2B). The slope of the data obtained by a linear fit gave a k_{11} value of 3.1 ± 0.3 ml/g for NIST mAb (Fig. 1B; green) which represent the mean and standard deviation from three repeat experiments. For golimumab the k_{11} value was 1.8 ± 0.3 ml/g (Fig. 2B; blue) also based upon three experiments. Rowe [41] has derived an expression for k_s values of uncharged, asymmetric macromolecules that involves an $(f/f_o)^3$ term. Typical f/fo values for mAbs are ~1.5. This predicts a k_s value for mAb of approximately 7–8 ml/g. The smaller self-nonideality k_s terms for these antibodies is an indicator of weak self-association (see below; [47,48]).

The cross-term nonideality for IgG and NIST mAb was measured by analyzing 100 nM FITC-IgG in unlabeled NIST mAb by AU-FDS (Fig. 1B; red). A linear fit of $1/s_{20,w}$ vs c gave a value of k_{31} = 2.9 ± 0.2 ml/g. For FITC-IgG sedimenting in Golimumab the k_{31} term was 1.7 ± 0.2 ml/g (Fig. 2B; red). The hydrodynamic nonideality exerted on IgG by the therapeutic antibodies was thus similar to the self-nonideality values as one might expect.

The cross-term nonideality of HSA sedimenting in the presence of the therapeutic antibodies also was investigated. 100 nM FITC-HSA was sedimented in concentrations of 1–12 mg/ml of NIST mAb. Plotting $1/s_{20,w}$ vs c in Fig. 1B (black) yielded a negative value of k_{21} = −1.2 ± 0.3. For the hydrodynamic cross-term nonideality of golimumab on 100 nM FITC-HSA, the $1/s_{20,w}$ vs c plot revealed a small cross-term nonideality k_{21} = 0.8 ± 0.3 ml/g (Fig. 2B; black). Above we suggested small mAb self-terms may reflect self-association effects. The small k_{21} values for mAb on HSA is more likely due to the mAb's faster sedimentation than HSA (6.5 s vs 4.4 s), resulting in the HSA boundary lagging behind the mAb boundary. Thus the albumin boundary does not feel the impact of high concentrations of NIST or

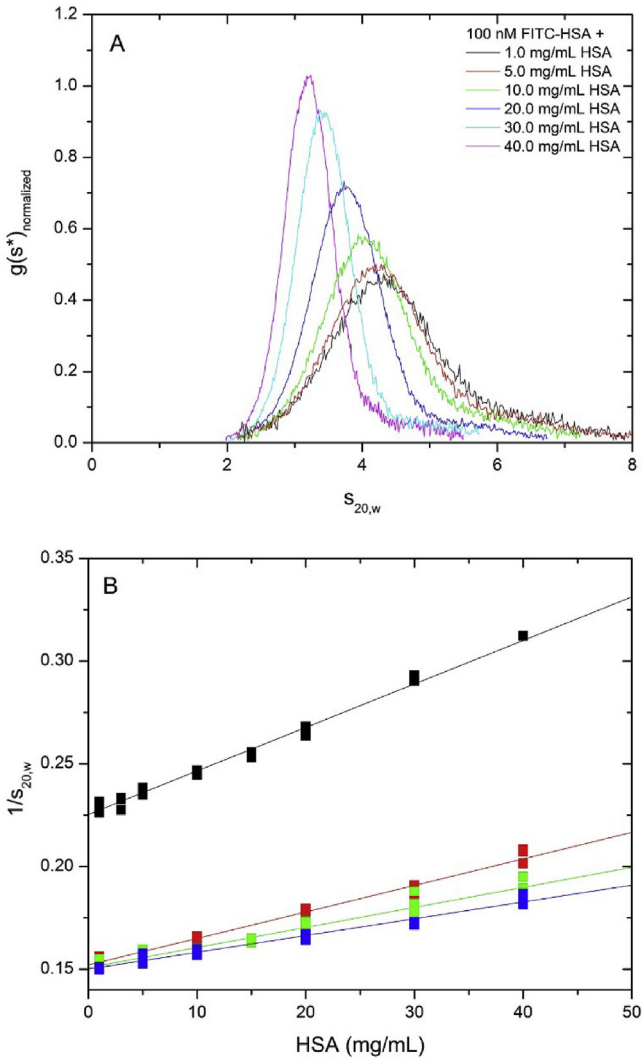

Fig. 3. (a) Normalized g(s*) distributions for 100 nM FITC-HSA as a function of HSA concentration. (b) Plotting the inverse of the monomer $s_{20,w}$ value of 100 nM FITC-HSA (black), FITC-IgG (red), Alexa-NIST mAb (blue), and Alexa-Golimumab (green) as a function of HSA concentration (1–40 mg/ml). The monomer $s_{20,w}$ values were determined from an A + B + C SEDANAL fit. The slope is equal to the magnitude of the hydrodynamic nonideality (k_s) divided by the sedimentation coefficient extrapolated to zero concentration (s^o).

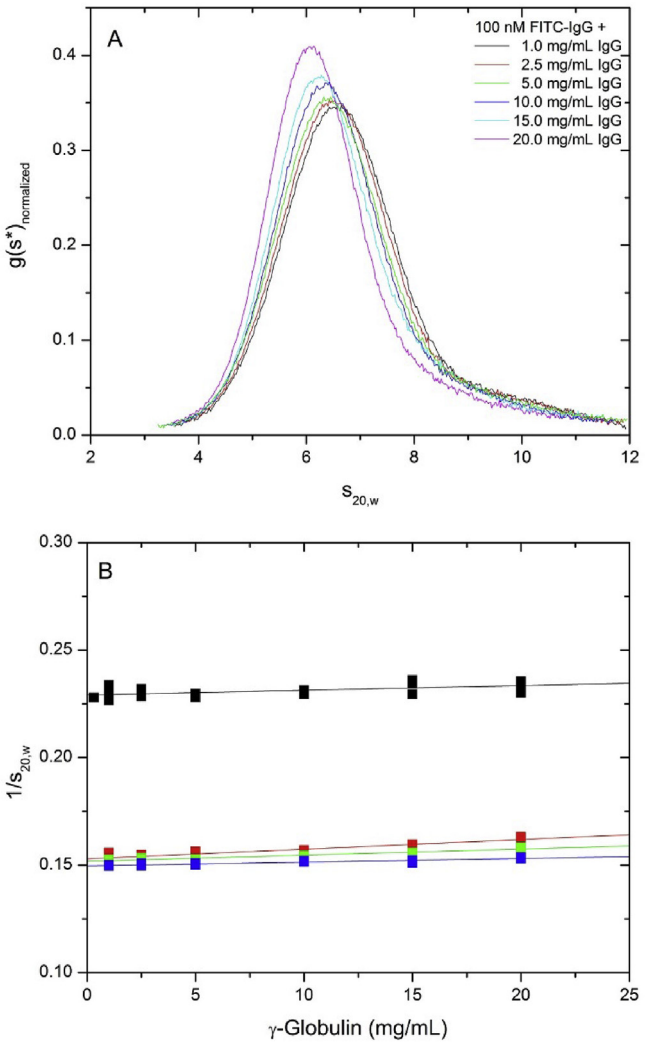

Fig. 4. (a) Normalized g(s*) distributions for 100 nM FITC-IgG as a function of IgG concentration. (b) Plotting the inverse of the monomer $s_{20,w}$ value of 100 nM FITC-HSA (black), FITC-IgG (red), Alexa-NIST mAb (green), and Alexa-Golimumab (blue) as a function of IgG concentration (1–20 mg/ml). The monomer $s_{20,w}$ values were determined from an A + B + C SEDANAL fit. The slope is equal to the magnitude of the hydrodynamic nonideality (k_s) divided by the sedimentation coefficient extrapolated to zero concentration (s^o).

golimumab once the boundaries have separated. Kingsbury and Laue [16] called this phenomena unmixing of co-solute complexes where the HSA boundary is not impacted by the variable density, viscosity and backflow of the mAb.[2]

The hydrodynamic properties of HSA were determined in the same manner. In order to obtain sedimentation data at physiologically relevant concentrations 100 nM FITC-HSA was sedimented in 1–40 mg/ml of HSA and monitored by AU-FDS. The g(s*) curves (Fig. 3A) indicate the HSA behaves as a nonideal monomer with small amounts of irreversible dimer and trimer present. The k_{22}, self-nonideality for HSA determined by linear fits of $1/s_{20,w}$ vs c plots, was 9.4 ± 0.2 ml/g (Fig. 3B; black).

The cross-term interaction parameter for 100 nM therapeutic antibodies and IgG were measured against increasing concentrations of HSA (1–40 mg/ml). The $1/s_{20,w}$ vs c plot for both NIST mAb (Fig. 3B; green) and golimumab (Fig. 3B; blue) reveal that HSA exerts greater nonideality on both antibodies than the antibodies did on themselves. HSA on NIST mAb gives a k_{12} = 6.5 ± 0.3 ml/g, and for golimumab k_{12} = 5.4 ± 0.2 ml/g. The hydrodynamic nonideality for HSA on IgG was determined to be 8.5 ± 0.3 ml/g. Thus HSA exhibits similar cross-term k_s effects on all three antibodies tested (NIST mAb, golimumab, and IgG).

Human IgG also was analyzed for self-nonideality. A slight shift to lower s values in the g(s*) distribution curves indicate nonideality at typical physiological concentrations of IgG (Fig. 4A). For IgG on IgG k_{33} = 2.9 ± 0.2 ml/g (Fig. 4B; red). The cross-term hydrodynamic nonideality between the therapeutic antibodies and IgG was measured with IgG as the background molecule at 1–20 mg/ml. For IgG on NIST mAb k_{13} = 1.9 ± 0.1 ml/g (Fig. 4B; green), and for IgG on golimumab k_{13} = 1.1 ± 0.1 ml/g (Fig. 4B; blue). While these values are similar, they are smaller than expected. IgG is much larger, more extended in shape, and heterogenous than HSA, all properties that should lead to larger hydrodynamic nonideality. Much like for the therapeutic antibodies, the flatness of the IgG curves (Fig. 4B) probably indicates weak self-association masking nonideality [47].

[2] In our previous work with ELP, IgG caused a deflection in the plateau that represented a buildup of ELP behind the faster moving IgG boundary [29]. We do not observe that phenomena with HSA and IgG.

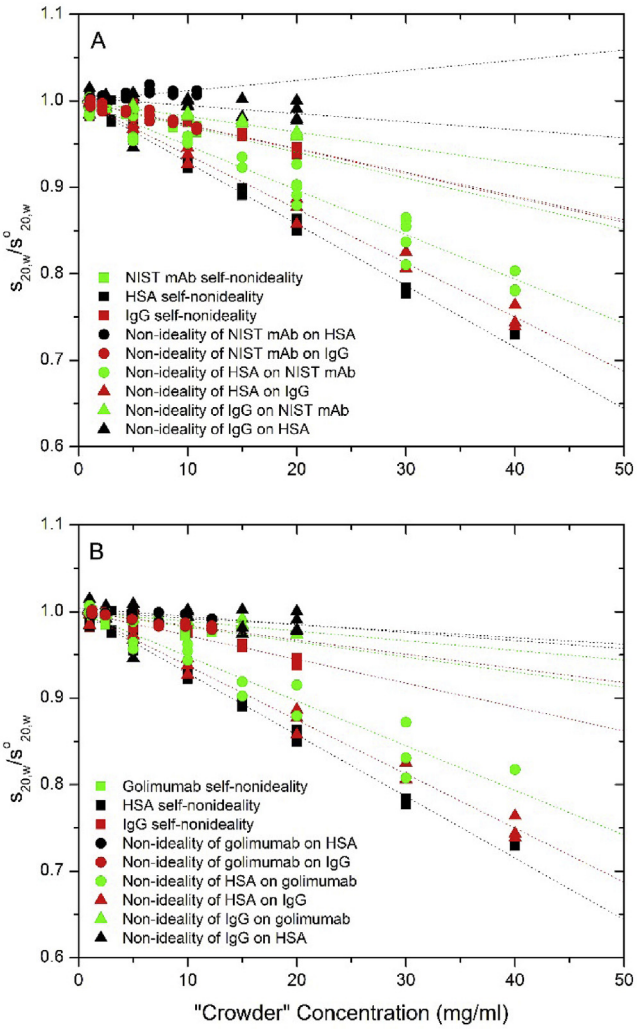

Fig. 5. Normalized plot of $s_{20,w}/s^{o}_{20,w}$ vs c for each component and interaction. The monomer $s_{20,w}$ value determined from an A + B + C SEDANAL fit was divided by the sedimentation coefficient extrapolated to zero concentration. This normalized all s vs concentration curves so that they extrapolate to 1. (a) NIST mAb (b) golimumab.

The hydrodynamic nonideality of IgG on HSA was also determined (Fig. 4B, black). The $1/s_{20,w}$ vs c plot reveals the effect of increasing amounts of IgG (1–20 mg/ml) on 100 nM FITC-HSA. The flat linear fit shows the weak non-ideality that is exerted on FITC-HSA with IgG as the background species. The k_{23} for this interaction was 1.0 ± 0.3 ml/g. As above this is most likely due to unmixing of co-solute complexes [16].

In Fig. 5, all of the sedimentation velocity data for NIST mAb and golimumab were normalized by dividing $s_{20,w}$ by s^{o} in order to have a common intercept of 1. These values were plotted versus the concentration of the appropriate crowder, or background molecule. This caused the data to separate into distinct groupings based on the non-ideality exerted by the background molecule. For example, the steepest slopes are where HSA was the background molecule. These curves show that HSA exerted the greatest hydrodynamic nonideality on itself and the three antibodies. All the self- and cross-term antibody data cluster in the next group consistent with these antibodies all behaving in a similar manner. The weakest effect is antibody on HSA. The hydrodynamic nonideality, k_s, values for the nine pair-wise interactions are summarized in a 3x3 matrix (Tables 1 and 2) as means ± standard deviation.

Global fitting in SEDANAL was also done for the self-nonideality terms. All six concentrations of a self-term experiment were fit globally in order to directly extract the k_s value from the data as opposed to linearly fitting a $1/s_{20,w}$ vs c plot. The k_s determined directly from SEDANAL fitting to an A + B + C + k_s model was similar for the self-nonideality measurements. The values shown are the mean ± sd from multiple data sets. The k_{22} for HSA was 8.2 ± 1.0 ml/g (mean ± sd from three data sets) compared to 9.4 ± 0.2 ml/g. The k_{33} self-nonideality for IgG was 3.1 ± 0.3 ml/g, similar to the 2.9 ± 0.2 ml/g value from the graphical approach. The k_{11} for NIST mAb was 4.2 ± 0.4 ml/g vs 3.1 ± 0.3 ml/g graphically. For Golimumab the k_{11} value was 2.5 ± 0.3 ml/g vs 1.8 ± 0.3 ml/g graphically. Thus, global analysis tends to yield similar k_s values to the $1/s_{20,w}$ vs c analysis. The concentrations of the unlabeled carrier protein were constrained in the same manner as the 1/s vs c plot. The major differences are that 1) SEDANAL direct boundary fitting is globally accounting for concentration dependence of all species, including dimers and trimers (albeit constrained to the same value on a weight basis), and 2) the convergence statistics include minimizing the residuals for ~120,000 raw data points directly. The cross-term k_s values for mAb-IgG and IgG-mAb pairs were also determined by global direct boundary fitting treating the data as if it were a self-nonideality term.[3] For IgG on NIST mAb (2.3 ± 0.04 ml/g vs 1.9 ± 0.1 ml/g) and golimumab (1.3 ± 0.2 ml/g vs 1.1 ± 0.1 ml/g) the results were similar. For experiments where the mAb was the carrier protein (NIST on IgG 4.4 ± 0.4 ml/g vs 2.9 ± 0.2 ml/g; golimumab on IgG 2.9 ± 0.1 ml/g vs 1.7 ± 0.2 ml/g) the results were still within a factor of 1.5–1.7. The cross-term k_s value involving HSA were not determined directly by global fitting because SEDANAL does not allow fitting the matrix elements due to their strong correlation.

To validate the k_s matrix SV experiments with Alexa-labeled mAb's were run with a mixture of HSA and IgG. This also serves as a serum mimic. The protein concentrations were run at a 2:1 ratio: 1, 5, 10, 20, 30, and 40 mg/ml HSA and 0.5, 2.5, 5, 10, 15, and 20 mg/ml IgG. These fits constrained the k_s matrix values and HSA and IgG concentrations, while floating s_1 and apparent extinction coefficients. A global fit for golimumab is shown in Fig. 6. The peak positions match exceptionally well, but the centrifugal region due to golimumab dimers is not well accounted for. Thus, the golimumab data was fit to a four species, non-interacting model (Fig. 7). In this fit the four species are Alexa-Golimumab, golimumab dimer, HSA, and IgG. The fourth species accounts for the 2–5% mAb dimer present while also accounting for the impact of HSA and IgG hydrodynamic nonideality. Fits of NIST mAb in mixtures of HSA and IgG gave equally good results (Fig. S2). To test the impact of estimating k_s by global direct boundary fitting, the data in Fig. 6 and S2 were refit with the values listed in parentheses in Table's 1 and 2. This is primarily a test of the IgG-mAb cross-terms which are within error identical (2.3 vs 1.9 for NIST and 1.3 vs 1.1 for golimumab). It also tests the impact of changes in HSA self-nonideality (8.2 vs 9.4) and indirectly HSA boundary shape on mAb sedimentation. Since HSA runs centripetal to mAbs this should be a minor effect. The refits are, not surprisingly, similar, with rms improving for golimumab (10.317–10.278) and getting slightly worse for NIST (11.798–11.876). As Fstat ratios these correspond to 0.99245 and 1.0133. This suggests the two methods, graphical and global fitting, are within error equally effective in describing the nonideality components of the data.

Sedimentation velocity experiments were then run in a dilution series of human serum. Normalized g(s*) curves from DCDT+ are shown for NIST mAb (Fig. S3) and golimumab (Fig. 8) in dilutions of human serum. A decrease in the $s_{20,w}$ value of the g(s*) distribution with increasing serum concentration shows significant nonideality. These data were also fit by SEDANAL to a A + Dimer + B + C + k_s

[3] This works because mAb and IgG all have similar molecular weights and sedimentation coefficients which approximate the boundary shapes equally well. For HSA-mAb or HSA–IgG cross-terms we would have to directly fit matrix elements, something that we have not currently allowed.

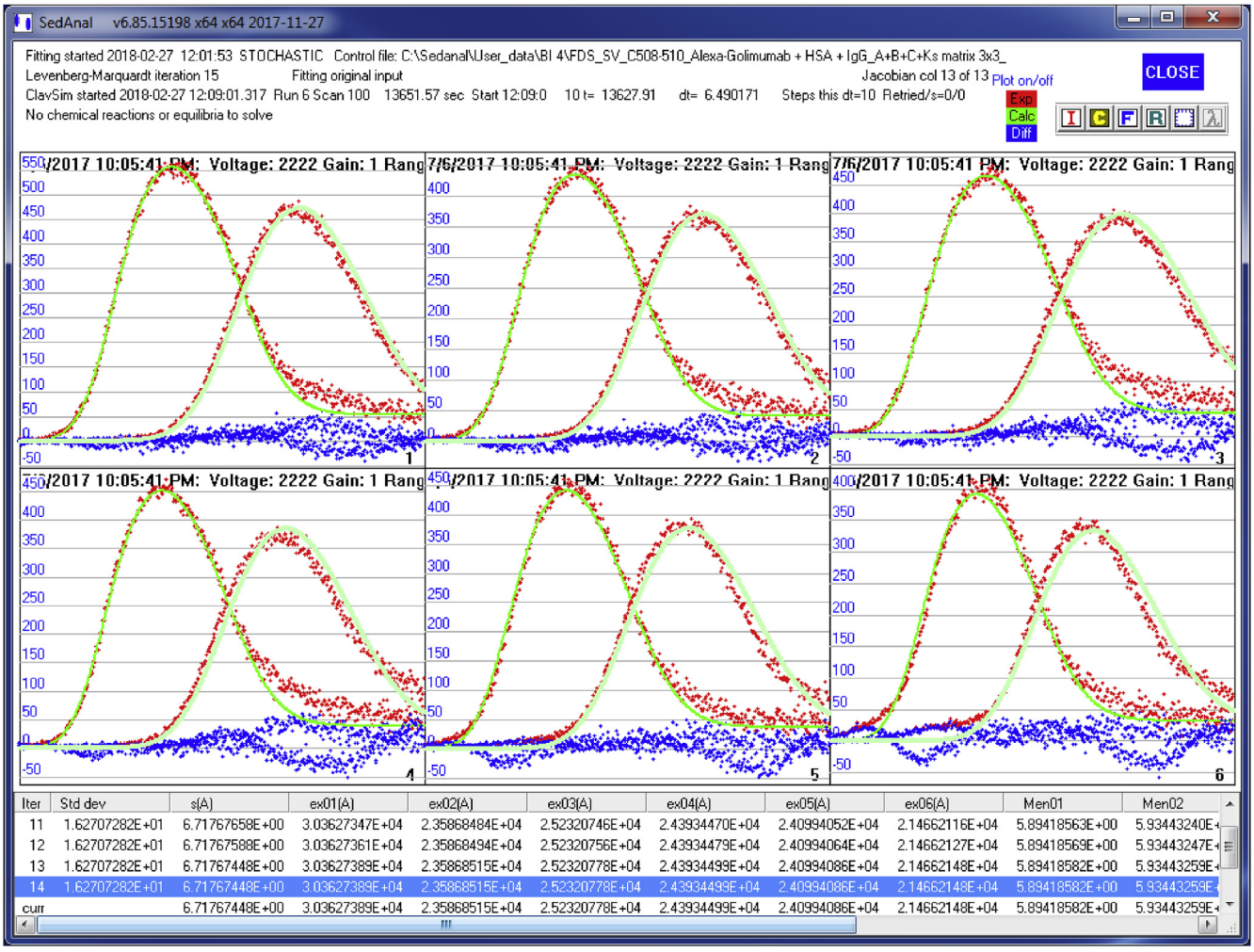

Fig. 6. SEDANAL fitting of sedimentation velocity data. 150 nM Alexa-Golimumab was run in 1–40 mg/ml HSA and 0.5–20 mg/ml IgG to mimic human serum. These data were fit to a three species, non-interacting model using a 3 × 3 k_s matrix (Table 2).

model with the 4 × 4 k_s matrix as part of the fitting model. The dimer component of the model accounts for the presence of irreversible dimers of therapeutic antibody. The concentrations of HSA and IgG in the serum were estimated by quantitative nonreducing SDS gels. Global fits revealed that the k_s matrices for all the pairwise interactions between major serum components and therapeutic antibodies qualitatively describe the data (Figs. 9 and S4). Deviations in the data at lower s values are caused by the presence of endogenous HSA (~4s) bound with bilirubin in the serum that produces its own detectable fluorescence signal. This was also observed in serum studies by Demeule et al. [5] but not in our ELP plus bovine serum studies [29].

Discussion

Rowe has repeatedly asserted that SV analysis on high concentration systems is “bound to fail” [17,41,49,50]. Simply running data sets through programs like SEDFIT to generate c(s) distributions generally will be uninformative. Absorbance at 280 nm is limited by Beers law and cannot be used to achieve the same ranges as tested in this high concentration study. Furthermore, absorbance detection fails, even in short solution path cells, where there are high concentration gradients that distort the absorbance readings [18,19]. We and others have observed refraction effects, peaks or dark bands where the light is refracted out of the optics, when trying to monitor tracer sedimentation at their excitation wavelengths. With interference optics, proper focusing at the 2/3 plane is critical. Even with proper focusing, steep concentration gradients cannot be followed by the current detectors.

To address these concerns, the AU-FDS method was introduced in 2004 [20] and because of the confocal optics, it was suggested that it would be appropriate to use with serum and cell extracts. A number of papers demonstrated that it worked very well [5,16,21,23] for extraction of qualitative data, but c(s) fitting consistently gives systematic residuals. Both Demeule et al. [5] and Kingsbury et al. [23] suggested it was not reasonable to do more than c(s) analysis, and that including the role of nonideality to allow a complete interpretation of the weakly associating nonideal data was not yet available. They both suggested there was still value in collecting data in serum that allows a broader application to drug discovery and fundamental mechanisms of pathology. For example, different complexes might form and this might impact the effectiveness of therapeutics [5].

Here we present AU-FDS tracer or BOLTS experiments [16,21,31–33] to study the hydrodynamic nonideality of therapeutic mAbs in the presence of high concentrations of two major serum proteins, HSA and total human IgG. The method is based upon the graphical extraction of hydrodynamic nonideality k_s from plots of monomer $1/s_{20,w}$ values vs concentration for pairwise interactions in a three component system. This produces nine phenomenological terms that are shown to describe the sedimentation of mAbs in high concentration mixtures of HSA and IgG. The verification of the k_s matrix involves global direct boundary fitting of tracer experiments run in mixtures of HSA and IgG with SEDANAL [27], an AUC software package that performs hydrodynamic modeling of complex

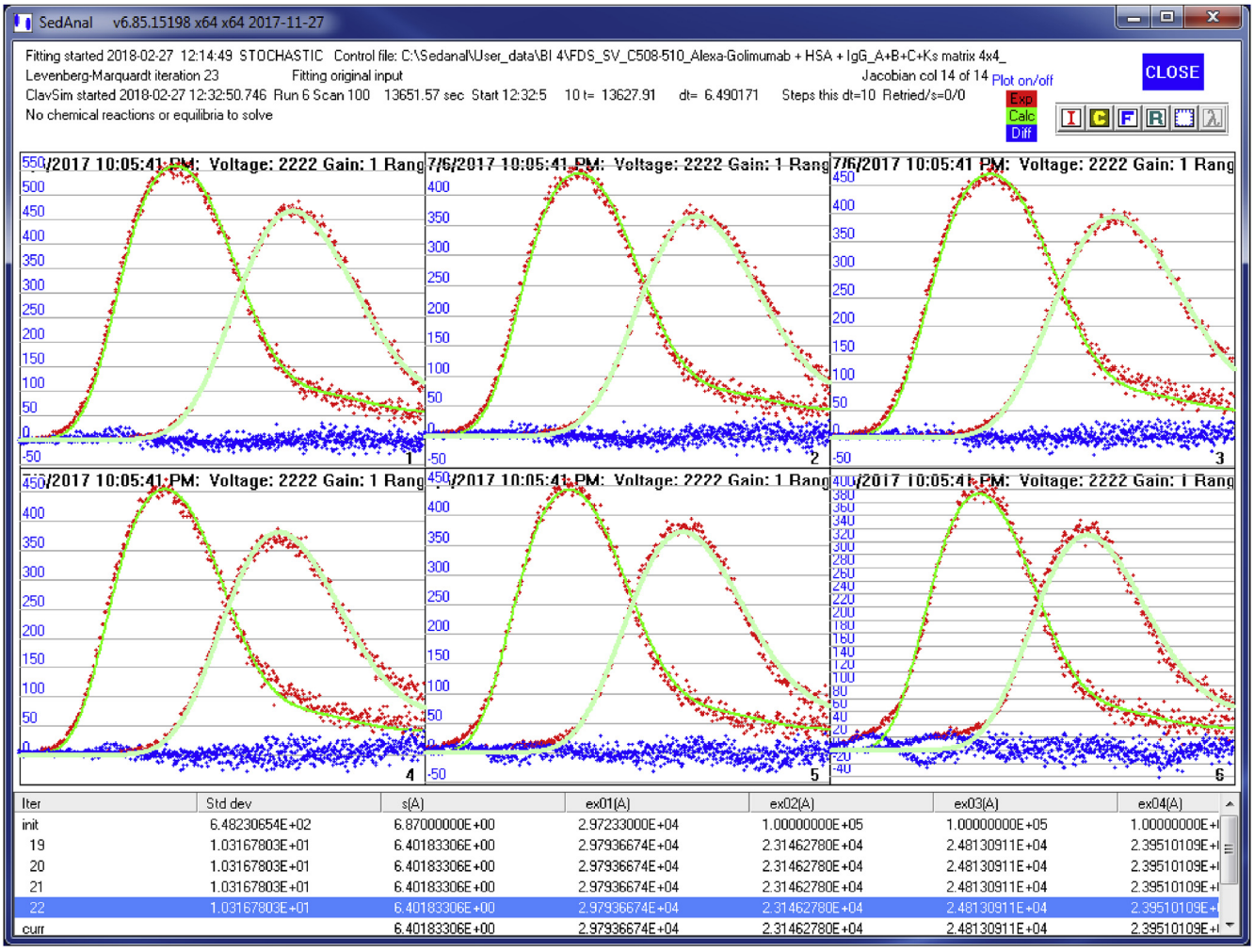

Fig. 7. SEDANAL fitting of sedimentation velocity data. 150 nM Alexa-Golimumab was run in 1–40 mg/ml HSA and 0.5–20 mg/ml IgG to mimic human serum. These data were fit to a four species, non-interacting model including mAb dimer and using an expanded 4 × 4 k_s matrix (Table 2, Fig. S1).

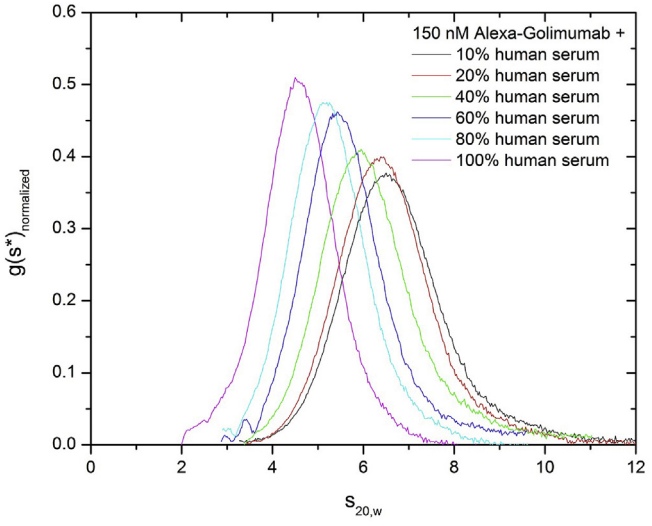

Fig. 8. Normalized g(s*) distributions of 150 nM Alexa-Golimumab as a function of human serum concentration (10–100%). The human serum dilutions were prepared with PBS.

sedimentation data. Including a fourth component, mAb dimeric aggregates, improves the fit. For antibodies that contain significant concentrations of larger aggregates, trimers and above, additional species may be appropriate. If we add trimers to the k_s matrix and float each cell separately, some but not all trimer/monomer ratios go to 1×10^{-6}, so we generally leave trimers out of the global ks fits.

The sedimentation coefficient used in the graphical approach was determined by fitting for the monomer s value to an A + B + C (monomer-dimer-trimer) non-interacting model in SEDANAL. The fitted s value of the monomer was then corrected to $s_{20,w}$. The sedimentation coefficient obtained from SEDANAL fitting was used instead of the weight-average sedimentation coefficient from DCDT$^+$ because fitting with SEDANAL is able to yield an s value for the monomeric protein that corresponds to the initial concentration conditions. The weight-average s value is not able to separate the different species present but rather is an average value of all species in solution at the time of the analysis. This leads to larger sedimentation coefficients but more importantly wide variability due to uncertainty in the integration range. It is generally assumed that concentration dependence for aggregates or oligomers, both k_s and $2BM_1$, are constant on a mass scale (ml/g). This is an empirical assumption because it is generally difficult to independently determine k_s values for all aggregates independently. The direct boundary SEDANAL fitting of self-nonideality data tests this empirical assumption by fitting to an A + B + C + k_s model where k_s is the same for all species. The results suggest reasonable agreement between graphical and global estimates of k_s (Tables 1 and 2), but future

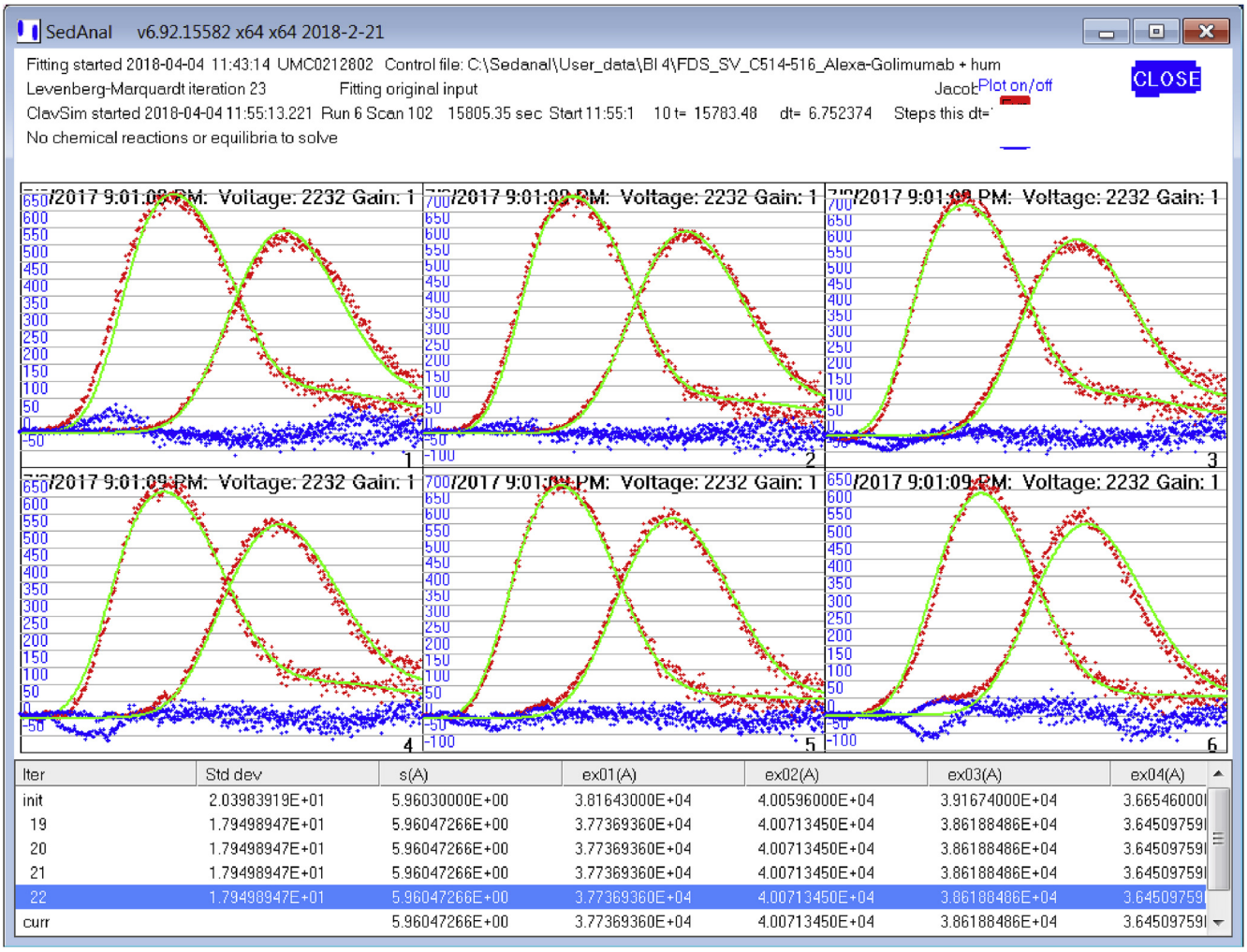

Fig. 9. SEDANAL fitting of sedimentation velocity data. 150 nM Alexa-Golimumab in 10%, 20%, 40%, 60%, 80%, and 100% human serum. These data were fit to a four species, non-interacting model including mAb dimer and using an expanded 4 × 4 k_s matrix (Table 2 and Fig. S1). The best fit includes fitting r_{men} and the dimer/monomer ratio for each sample.

studies will test the constant k_s assumption.

Repulsive nonideality (B > 0, k_s > 0) results from excluded volume and charge effects. Solution backflow is caused by excluded volume of the effective hydrodynamic radius of the sedimenting macromolecules. As a molecule sediments through solution it displaces solvent. The displaced solvent then flows backwards slowing the sedimentation of all other species in the vicinity. At high macromolecule concentrations, more solvent must backflow. This phenomena was studied extensively during the early development of AUC methods [51–54]. Numerous studies have also looked at the theoretical basis for hydrodynamic nonideality [17,41,42,49,50,55,56]. There is general agreement between measurements and theory for spherical, uncharged macromolecules. Globular or spherical molecules as different in size as BSA [57] and Bushy Stunt Virus, BSV [58], give k_s values of 5–8 ml/g. Species with higher frictional ratios due to extended structures are prone to exhibiting greater nonideality because they carry entrained and weakly bound solvent with them. Rowe (41) has proposed a general equation that corrects for shape through a $(f/f_o)^3$ term;

$$ks = 2v\left[\frac{Vs}{v} + \left(\frac{f}{fo}\right)^3\right]$$

where Vs is swollen volume and v is vbar. Our antibodies have experimental f/f_o values of 1.50–1.53. Using a v of 0.73 and a Vs/v ratio of 1.4 for globular proteins [59], corresponds to a calculated k_s range for uncharged mAbs of 7–7.3. A more realistic swollen volume ratio Vs/v, 3.3–3.5 [60], gives a mAb range for k_s of 9.8–10.2.

All of the self- and cross-term IgG or mAb k_s values measured here are in the range of 1.1–3.1 ml/gm with an average value of 2.29 ± 0.75 ml/g. For NIST the average is 2.7 ± 0.54 ml/g; for Golimumab the average is 1.87 ± 0.75 ml/g. Similar results have been obtained by Yang et al. [47] on seven mAbs from different classes of IgG with average self-k_s values of ~4.6 ml/g. Both our work and their studies are consistent with the presence of weak association that masks or lowers the magnitude of k_s. Yang et al. [47] tested this hypothesis by raising the PBS salt concentration from 150 to 500 mM. This raised the k_s values of the two mAbs tested significantly, consistent with suppression of charge mediated self-association. Alternatively, we fit the mAb data to a nonideal associating model (k_s + K_2) by direct boundary fitting with SEDANAL. For NIST the average K_2 is 1435 ± 118 M^{-1} with an average k_s increased from 3.1 to 10.9 ± 0.7 ml/gm; for golimumab the average K_2 is 1096 ± 262 M^{-1} with an average k_s increased from 1.8 to 7.9 ± 0.9 ml/gm. This confirms the masking hypothesis; when unaccounted for in the model, the presence of association lowers the apparent k_s value. However, these experiments were only conducted up to 12 mg/ml (~80 μM) while these K_2 values correspond to 700–900 μM. There is large cross correlation (R = ~0.96; Fig. S5) and uncertainty in these values and this model. For example, we assume dimers as the simplest model, but higher order oligomers are likely to form [47,48]. Furthermore, if we add

thermodynamic nonideality $2BM_1$ to the model it returns values of zero in the majority of fits. This applies to $k_s + 2BM_1$ fit and to k_s, $2BM_1 + K_2$ fits.[4] Recently, using similar AUC methods, Hopkins et al. [48] report similar results with mAbs that exhibit a range of association strengths and stoichiometries up to hexamer.

To address this, AU-FDS simulations were done on mAbs samples from 1 to 10 mg/ml with $k_s = 8.5$ ml/gm, $2BM_1 = 5$ ml/gm and $K_2 = 3000\ M^{-1}$ and comparable noise levels. Dimer and trimer aggregates were also included in the modeling. Fits correctly returned all the parameters with excellent uncertainty by bootstrap with replacement ($k_s = 8.5 \pm 0.04$; $2BM_1 = 4.98 \pm 0.46$; $K_2 = 3006 \pm 20$). Accurate BM_1 fitting of simulated data suggests some additional uncertainty is present in our experimental AU-FDS tracer data, due to either sample heterogeneity or signal bias. While exploring these issues, we also performed synthetic boundary experiments to test the possibility of extracting $2BM_1$ from diffusion measurements [30]. This is based upon the presence of both hydrodynamic and thermodynamic nonideality in diffusion:

$$D = \frac{D^o(1 + 2BMc)}{(1 + k_s c)}$$

We plot $D(1 + k_s c)$ vs concentration and extract the $2BM_1$ term from the slope of the plot [30]. As with the k_s measurements reported here, association impacts the sign and magnitude of $2BM_1$ measurements [30]. In addition we have performed SV experiments over a wider concentration range, up to 120 mg/ml on HSA and IgG. This revealed that above ~60 mg/ml the 1/s vs c plot is nonlinear and requires a second order correction term k_{s2} of ~0.01 $(ml/g)^2$. This introduces additional parameter correlation and uncertainty. Results on higher concentration data along with successful implementation of nonideality theory from Todd and Haschemeyer [61] will be presented elsewhere.

Kingsbury et al. [23] also questioned the difficulty of interpreting AU-FDS data from heterogeneous solutions. The components undergo unmixing of co-solute complexes which creates multiple concentration gradients, and variability in density and viscosity throughout the radial dimensions. Our approach addresses many of these issues, in part, by modeling the unlabeled carrier protein during the fitting, by taking into account both nonideality through the k_s matrix, and hetero-interactions between labeled and unlabeled material, through appropriate association schemes. Thus, rather than extracting c(s) or g(s) distribution peaks, we model the influence of nonideality and both self- and hetero-association. More detailed studies of these problems, including reaction stoichiometry and radial and time variable density, are in preparation.

Yang et al. [47] measured the charge on their mAbs and found a remarkably narrow valance range near −6.3, due presumably to charge buffering by ion binding. The major effect of high salt concentration was to raise the apparent value of k_s by suppressing macromolecular association. Nonetheless, highly charged molecules experience nonideality through charge repulsion and their effective ionic radius [62,63]. In a solution environment with low salt concentration the sedimentation of a charged molecule is also slowed due to the primary charge effect [64]. This is the reason sufficient salt (100 mM) is usually added for proper biophysical investigations. With highly charged macromolecules (DNA, IDPs), charge effects may still be evident under high salt conditions [65,66]. Thermodynamic nonideality is well understood in terms of Donnan equilibrium, even for self-associating systems [65], and highly appropriate for application to sedimentation equilibrium studies. It is certainly well appreciated that charge effects in high concentration regime will influence hydrodynamic nonideality [21,67,68]. When we account for association in the fitting model, the k_s value for NIST mAb increases to ~11, in the upper range of calculated value for an uncharged antibody. Future work is required to address the role of charge and salt binding in AU-FDS high concentration hydrodynamic measurements.

The use of fluorescence optics in high concentration serum studies raises many potential concerns about linearity, signal quenching, inner filter effects and contamination [37,69]. It is now well established that the AU-FDS system is linear up to ~500 nM [16,37]. Thus we and others recommend working with labeled samples at 100–200 nM and below while varying the unlabeled carrier material to test for concentration dependence. The ability of Lamm solution modeling to accurately fit the SV data suggests the absence of quenching, otherwise the signal would drop faster than radial dilution, and would be evident in the residuals (Figs. 7 and S2). Contamination in serum samples is widely but not universally reported. We see two peaks ~50 counts in our serum samples at 2s and 4s. We suspect the 4s peak to be bilirubin bound to HSA; we suspect the 2s peak is HDL or an HSA fraction with bound fatty acids (Tom Laue, private communication). The presence of these peaks is also the reason we prefer to work with 100–200 nM F-mAb's at sufficient gain to have signals in the 1000's, thus making the spurious signals minor issues. One can account for these peaks by adding them to the model, but studies at sub-nM concentrations in serum may be a challenge. Labeling HSA is also a potential problem because serum albumin tends to bind fluorescent compounds non-covalently. We have observed this in our low speed synthetic boundary studies where we must account for a free fluorophore in the analysis of HSA diffusion measurements [30]. We have also observed free fluorescent dye falling off of the HSA and binding to a carrier antibody leading to the detection of two separate boundaries. All of these concerns can be dealt with through the ModelEditor in SEDANAL, but one must be aware of the additional challenges AU-FDS potentially provides. Furthermore, while the data on mAb in serum dilutions (Figs. 9 and S4) are qualitatively encouraging, there are still systematics in the residuals that future investigations will hopefully be able to address.

Conclusions

Here we demonstrate the use of AU-FDS optics to study the hydrodynamic nonideality of therapeutic antibodies in high concentrations of serum proteins. The approach uses tracer amounts of labeled mAbs and high concentration solutions of HSA, human IgG or dilutions of serum directly. The analysis described is implemented by either graphical methods or by direct boundary fitting with SEDANAL. The results reveal that antibodies all display a weak tendency to self- and hetero-associate which masks hydrodynamic nonideality. SEDANAL fitting to complex models involving k_s, BM_1 and association schemes can be successfully implemented to extract these parameters if high enough carrier protein concentrations are tested. The method has broad application to the characterization of antibodies and other protein-based therapeutics, especially in the further evaluation of lead candidates and biosimilars.

Acknowledgements

Supported by Boehringer-Ingelheim and UMC AUC Facility. This work was presented at the 23rd International AUC Workshop and Symposium, Glasgow, Scotland. We thank Dave Bain, Tom Laue and Sharon Lobert for constructive comments. We thank Danlin Yang for her many rigorous and extensive parallel experimental results on a matrix of 12 recombinantly produced mAbs and pooled γ-globulins samples that validate our results. We thank Dave Bain and his collaborators for sharing their results prior to publication. We especially thank Tom Laue for creating the FDS system and encouraging research efforts in high concentration hydrodynamic biophysics.

[4] It is worth noting that hydrodynamic fitting of nonideal sedimentation velocity data has severe computational challenges that were outlined by Todd and Haschemeyer [61]. Our next publication will address many of these issues.

Appendix A. Supplementary data

Supplementary data related to this article can be found at http://dx.doi.org/10.1016/j.ab.2018.04.002.

References

[1] S.J. Shire, Z. Shahrokh, J. Liu, Challenges in the development of high protein concentration formulations, J. Pharmacol. Sci. 93 (2004) 1390–1402.
[2] S. Berkowitz, J.R. Engen, J.R. Mazzeo, G.B. Jones, Analytical tools for characterizing biopharmaceuticals and the implications for biosimilars, Nat. Rev. Drug Discov. 11 (7) (2013) 527–540.
[3] S.A. Berkowitz, Role of analytical ultracentrifugation in assessing the aggregation of protein biopharmaceuticals, AAPS J. 8 (3) (2006) E590–E605.
[4] M. Haberger, et al., Rapid characterization of biotherapeutic proteins by size-exclusion chromatography coupled to native mass spectrometry, mAbs 8.2 (2016) 331–339.
[5] B. Demeule, S.J. Shire, J. Liu, A therapeutic antibody and its antigen form different complexes in serum than in phosphate-buffered saline: a study by analytical ultracentrifugation, Anal. Biochem. 388 (2009) 279–287.
[6] T. Arakawa, J.S. Philo, D. Ejima, K. Tsumoto, F. Arisaka, Aggregation analysis of therapeutic proteins, Part 1, BioPro. Inter 4 (10) (2006) 42–49.
[7] T. Arakawa, J.S. Philo, D. Ejima, K. Tsumoto, F. Arisaka, Aggregation analysis of therapeutic proteins, Part 2, BioPro. Inter 5 (4) (2007) 36–47.
[8] T. Arakawa, J.S. Philo, D. Ejima, K. Tsumoto, F. Arisaka, Aggregation analysis of therapeutic proteins, Part 3, BioPro. Inter 5 (4) (2007) 52–70.
[9] J.P. Gabrielson, K.K. Arthur, B.S. Kendrick, T.W. Randolph, M.R. Stoner, Common excipients impair detection of protein aggregates during sedimentation velocity analytical ultracentrifugation, Biotec 98 (2009) 50–62.
[10] S. Kozlowski, J. Woodcock, K. Midthun, R.B. Sherman, Developing the nation's biosimilars program, N. Engl. J. Med. 365 (2011) 385–388.
[11] J. Woodcock, et al., The FDA's assessment of follow-on protein products: a historical perspective, Nat. Rev. Drug Discov. 6 (2007) 437–442 PubMed: 17633790.
[12] S.A. Berkowitz, J.S. Philo, Characterizing biopharmaceuticals using analytical ultracentrifugation, in: D.J. Houde, S.A. Berkowitz (Eds.), Biophysical Characterization of Proteins in Developing Biopharmaceuticals, Elsevier Inc, 2015, pp. 211–260.
[13] K.K. Arthur, J.P. Gabrielson, B.S. Kendrick, M.R. Stoner, Detection of protein aggregates by sedimentation velocity analytical ultracentrifugation (SV-AUC): sources of variability and their relative importance, J. Pharmacol. Sci. 98 (10) (2009) 3522–3539.
[14] H. Zhao, R. Ghirlando, C. Alfonso, P. Schuck, A multilab comparison of calibration accuracy and the performance of external references in analytical ultracentrifugation, PLoS One 10 (2015) e0126420.
[15] K.K. Arthur, B.S. Kendrick, J.P. Gabrielson, Guidance to achieve accurate aggregate quantitation in biopharmaceuticals by SV-AUC, in: B. Imperiali (Ed.), Methods in Enzymology, Elsevier Inc., 2015, pp. 477–500.
[16] J.S. Kingsbury, T.M. Laue, Fluorescence-detected sedimentation in dilute and highly concentrated solutions, Meth. Enzymol. 492 (2011) 283–304.
[17] T.D.M. Besong, A.J. Rowe, Acquisition and analysis of data from high concentration solutions, in: S. Uchiyama, F. Arisaka, W.F. Stafford, T. Laue (Eds.), Analytical Ultracentrifugation: Instrumentation, Software, and Applications, Springer, Japan KK, 2016, pp. 499–519.
[18] R. Dhami, H. Cölfen, S.E. Harding, A comparative “Schlieren” study of the sedimentation behaviour of three polysaccharides using the Beckman Optima XL-A and Model E analytical ultracentrifuge, Progr. Collloid Polym. Sci. 99 (1995) 187–192.
[19] H. Cölfen, S.E. Harding, A study on Schlieren patterns derived with the Beckman Optima XL-A UV-absorption optics, Prog. Colloid Polym. Sci. 99 (1995) 167–186.
[20] I.K. Macgregor, A.L. Anderson, T.M. Laue, Fluorescence detection for the XLI analytical ultracentrifuge, Biophys. Chem. 108 (1–3) (2004) 165–185.
[21] R.R. Kroe, T.M. Laue, NUTS and BOLTS: applications of fluorescence-detected sedimentation, Anal. Biochem. 390 (1) (2009) 1–13.
[22] P. Schuck, Size-distribution analysis of macromolecules by sedimentation velocity ultracentrifugation and Lamm equation modeling, Biophys. J. 78 (2000) 1606–1619.
[23] J.S. Kingsbury, T.M. Laue, E.S. Klimtchuk, R. Théberge, C.E. Costello, L.H. Connors, The modulation of transthyretin tetramer stability by cysteine 10 adducts and the drug diflunisal: direct analysis by fluorescence-detected analytical ultracentrifugation, J. Biol. Chem. 283 (18) (2008) 11887–11896.
[24] W.F. Stafford, Boundary analysis in sedimentation transport experiments: a procedure for obtaining sedimentation coefficient distributions using the time derivative of the concentration profiles, Anal. Biochem. 203 (1992) 295–301.
[25] J.S. Philo, Improved methods for fitting sedimentation coefficient distributions derived by time-derivative techniques, Anal. Biochem. 354 (2006) 238–246.
[26] W.F. Stafford, E.H. Braswell, Sedimentation velocity, multi-speed method for analyzing polydisperse solutions, Biophys. Chem. 108 (2004) 273–279.
[27] W.F. Stafford, P.J. Sherwood, Analysis of heterologous interacting systems by sedimentation velocity: curve fitting algorithms for estimation of sedimentation coefficients, equilibrium and kinetic constants, Biophys. Chem. 108 (1–3) (2004) 231–243.
[28] W.F. Stafford, Analysis of nonideal, interacting and noninteracting systems by sedimentation velocity analytical ultracentrifugation, in: S. Uchiyama, F. Arisaka, W.F. Stafford, T. Laue (Eds.), Analytical Ultracentrifugation: Instrumentation, Software, and Applications, Springer, Japan KK, 2016, pp. 463–482.
[29] J.J. Correia, D.F. Lyons, P. Sherwood, W.F. Stafford, Techniques for dissecting the Johnston-Ogston effect, in: S. Uchiyama, F. Arisaka, W.F. Stafford, T. Laue (Eds.), Analytical Ultracentrifugation: Instrumentation, Software, and Applications, Springer, Japan KK, 2016, pp. 483–497.
[30] R.T. Wright, D. Hayes, P.J. Sherwood, W.F. Stafford, J.J. Correia, AUC measurements of diffusion coefficients of monoclonal antibodies in the presence of human serum proteins, Eur. Biophys. J. (2018) (in press).
[31] G. Rivas, A.P. Minton, Tracer sedimentation equilibrium: a powerful tool for the quantitative characterization of macromolecular self- and hetero-associations in solution, Biochem. Soc. Trans. 31 (2003) 1015–1019.
[32] G. Rivas, A.P. Minton, Non-ideal tracer sedimentation equilibrium: a powerful tool for the characterization of macromolecular interactions in crowded solutions, J. Mol. Recogn. 17 (2004) 362–367.
[33] G. Rivas, A.P. Minton, Beyond the second virial coefficient: sedimentation equilibrium in highly non-deal solutions, Methods 54 (1) (2011) 167–174.
[34] S. Liu, W.F. Stafford, An optical thermometer for direct measurement of cell temperature in the Beckman instruments XL-A analytical ultracentrifuge, Anal. Biochem. 224 (1995) 199–202.
[35] D.B. Hayes, J.P. Philo, T.M. Laue, Sednterp: Interpretation of Sedimentation Data Version 1.X. 2000 Lines of Visual Basic Code, Written for Windows 3.X.
[36] T.M. Laue, B.D. Shah, T.M. Ridgeway, S.L. Pelletier, Computer-Aided Interpretation of analytical sedimentation data for proteins, in: S.E. Harding, A.J. Rowe, J.C. Horton (Eds.), Analyical Ultracentrifugation in Biochemistry and Polymer Sciences, Royal Academy of Sciences, 1992, pp. 90–125.
[37] D.F. Lyons, J.W. Lary, B. Husain, J.J. Correia, J.L. Cole, Are fluorescence-detected sedimentation velocity data reliable? Anal. Biochem. 437 (2) (2013) 133–137.
[38] M.F. Bailey, L.M. Angley, M.A. Perugini, Methods for sample labeling and meniscus determination in the fluorescence-detected analytical ultracentrifuge, Anal. Biochem. 390 (2009) 218–220.
[39] J.P. Johnston, A.G. Ogston, A boundary anomaly found in the ultracentrifugal sedimentation of mixture, Trans. Faraday Soc. 42 (1946) 789–799.
[40] P.J. Sherwood, W.F. Stafford, SEDANAL: model = -dependent and model-independent analysis of sedimentation data, in: S. Uchiyama, F. Arisaka, W.F. Stafford, T. Laue (Eds.), Analytical Ultracentrifugation: Instrumentation, Software, and Applications, Springer, Japan KK, 2016, pp. 81–102.
[41] A.J. Rowe, The concentration dependence of transport processes: a general description applicable to sedimentation, translational diffusion, and viscosity coefficients of macromolecular solutes, Biopolymers 16 (1977) 2595–2611.
[42] S.E. Harding, P. Johnson, The concentration-dependence of macromolecular parameters, Biochem. J. 231 (1985) 543–547.
[43] S.E. Harding, P. Johnson, Physiochemical studies on turnip-yellow-mosaic virus: homogeneity, relative molecular masses, hydrodynamic radii and concentration-dependence of parameters in non-dissociating solvents, Biochem. J. 231 (1985) 549–555.
[44] A. Solovyova, P. Schuck, L. Costenaro, C. Ebel, Non-ideality by sedimentation velocity of Halophilic Malate Dehydrogenease in complex solvents, Biophys. J. 81 (2001) 1868–1880.
[45] A. Saluja, R.M. Fesinmeyer, S. Hogan, D.N. Brems, Y.R. Gokarn, Diffusion and sedimentation onteraction parameters for measuring the second virial coefficient and their utility as predictors of protein aggregation, Biophys. J. 99 (2010) 2657–2665.
[46] S. Yadav, T.M. Scherer, S.J. Shire, D.S. Kalonia, Use of dynamic light scattering to determine second virial coefficient in a semidilute concentration regime, Anal. Biochem. 411 (2011) 292–296.
[47] D. Yang, J.J. Correia, W.F. Stafford, C.J. Roberts, S. Singh, D. Hayes, R. Kroe-Barrett, A. Nixon, T.M. Laue, Weak IgG interactions in high concentration homo- and hetero- IgG backgrounds characterized by fluorescence analytical ultracentrifugation, Protein Sci. (2018) (in press).
[48] M.M. Hopkins, C.M. Lambert, J.S. Bee, A. Parupudi, D.L. Bain, Determination of interaction parameters for reversibly self-associating antibodies: a comparative analysis, J. Pharmacol. Sci. (2018) (in press).
[49] T.R. Patel, S.E. Harding, A. Ebringerova, M. Deszczynski, Z. Hromadkova, A. Togola, B.S. Paulsen, G.A. Morris, A.J. Rowe, Weak self-association in a carbohydrate system, Biophys. J. 93 (2007) 741–749.
[50] A.J. Rowe, Ultra weak reversible protein-protein interactions, Methods 54 (2011) 157–166.
[51] G. Kegeles, F.J. Gutter, The determination of sedimentation constants from Fresnel diffraction patterns, JACS 73 (1951) 3770–3777.
[52] H.K. Schachman, W.F. Harrington, Ultracentrifuge studies with a synthetic boundary cell. I. General applications, J. Polym. Sci. 12 (1954) 379–390.
[53] R. Hersh, H.K. Shachman, Ultracentrifuge studies with a synthetic boundary cell, J. Am. Chem. Soc. 77 (1955) 5228–5234.
[54] R. Hersh, H.K. Schachman, Ultracentrifuge studies with a synthetic boundary cell. III. Sedimentation of a slow component in the presence of a faster species, J. Phys. Chem. 62 (1958) 170–171.
[55] G.K. Batchelor, Sedimentation in a dilute dispersion of spheres, J. Fluid Mech. 52 (1972) 245–268.
[56] A.J. Rowe, The concentration dependence of sedimentation, in: S.E. Harding, A.J. Rowe, J.C. Horton (Eds.), Analytical Ultracentrifugation in Biochemistry and Polymer Science, Royal Society of Chemistry, 1992, pp. 394–406.
[57] R.L. Baldwin, Boundary spreading in sedimentation-velocity experiments 5. Measurements of the diffusion coefficient of bovine albumin by Fujita's equation, Biochem. J. 65 (1957) 503–512.
[58] W.F. Harrington, H.K. Schachman, Analysis of a concentration anomaly in the ultracentrifuge of mixtures, J. Am. Chem. Soc. 75 (1953) 3533–3539.
[59] D.C. Teller, Accessible area, packing volumes and interaction surfaces of globular proteins, Nature 260 (1976) 729–731.

[60] J.M. Creeth, C.G. Knight on the estimation of the shape of macromolecules from sedimentation and viscosity measurements, BBA 102 (1965) 549–558.
[61] G.P. Todd, R.H. Haschemeyer, General solutions to the inverse problem of the differential equation of the ultracentrifuge, Proc. Natl. Acad. Sci. Unit. States Am. 78 (1981) 6739–6743.
[62] L. Onsager, R.W. Fuoss, Irreversible processes in electrolytes diffusion, conductance, and viscous flow in arbitrary mixtures of strong electrolytes, J. Phys. Chem. 36 (1932) 2689–2778.
[63] R.W. Fuoss, The velocity field in electrolytic solutions, J. Phys. Chem. 63 (4) (1959) 633–636.
[64] K.O. Pedersen, On charge and specific ion effects on sedimentation in the ultracentrifuge, J. Phys. Chem. 62 (10) (1958) 1282–1290.
[65] D.E. Roark, D.A. Yphantis, Equilibrium centrifugation of nonideal systems. The Donnan effect in self-associating systems, Biochemist 10 (1972) 3241–3249.
[66] S.S. Margossian, W.F. Stafford, Calcium-induced dimerization of troponin-C, J. Mol. Biol. 257 (1980) 1160–1165.
[67] T. Laue, Proximity energies: a framework for understanding concentrated solutions, J. Mol. Recogn. 25 (2012) 165–173.
[68] T. Laue, B. Demeler, A framework for postredictionist protein biochemistry, Nat. Chem. Biol. 7 (2011) 1–4.
[69] S.K. Chaturvedi, H. Zhao, P. Schuck, Sedimentation of reversibly interacting macromolecules with changes in fluorescence quantum yield, Biophys. J. 112 (2012) 1374–1382.